Sonochemical and mechanochemical synthesis of iron-based nano-hydrotalcites promoted with Cu and K as catalysts for CO and CO_2 Fischer-Tropsch synthesis

Arian Grainca[a], Elisa Boccalon[b], Morena Nocchetti[c*], Riccardo Vivani[c], Alessandro Di Michele[d*], Mariangela Longhi[a], Carlo Pirola[a]

[a]*Università degli Studi di Milano, Dipartimento di Chimica, Via Golgi 19, 20133 Milano (Italy)*
[b] *Università degli Studi di Perugia, Dipartimento di Chimica, Biologia e Biotecnologie, Via Elce di Sotto 8, 06123 Perugia (Italy)*
[c] *Università degli Studi di Perugia, Dipartimento di Scienze Farmaceutiche, Via del Liceo, 06123 Perugia (Italy)*
[d] *Università degli Studi di Perugia, Dipartimento di Fisica e Geologia, Via Pascoli, 06123 Perugia (Italy)*

**Corresponding authors: alessandro.dimichele@unipg.it – morena.nocchetti@unipg.it*

Abstract

A novel class of Fe-based nano hydrotalcites as catalysts for Fischer-Tropsch (FT) synthesis, with a focus on CO_2 hydrogenation have been prepared, characterized and tested. These catalysts were synthesized using two green, energy- and time-saving synthesis methods: ultrasound-assisted co-precipitation and solvent-free mechanochemical syntesis. The catalysts demonstrate very satisfactory CO and CO_2 conversion capacities, in particular with good selectivities towards heavy hydrocarbons. The ultrasound-processed variant is particularly noteworthy, displaying about 10% higher activity under specific conditions. The unique physicochemical properties of these catalysts, which were extensively characterized by XRD, TGA, (ATR) FT-IR, ICP-OES, SEM, TEM, BET, and TPR, are responsible for their remarkable potential for CO and CO_2 conversion with varied product distribution. These findings highlight as these iron-based hydrotalcites can be considered as a new promising class of catalyst for CO and CO_2 conversion by Fischer-Tropsch reaction.

Keywords: Fischer Tropsch; Hydrotalcite; Iron; CO_2 conversion; Ultrasound; Ball milling.

1. Introduction

The need to replace fuels and chemicals derived from refining and converting crude oil is driving the development of industrial processes using alternative sources [1]. Fischer Tropsch synthesis (FT) is a well-established industrial process that can be adapted to meet these needs. For instance, by using syngas (mixture of H_2 and CO) manufactured from CH_4, coal or, as a new trend, biomass [2]. The FT process converts syngas into hydrocarbons in the C_1 to C_{100} range. Common catalysts used for the synthesis are iron-, cobalt- or ruthenium-based, and the resulting products span from hydrocarbon fuels (such as gasoline, diesel fuel and jet fuel) to olefins, waxes, and oxygenated compounds like alcohols. The synthesis, in a nutshell, consists of two main reactions: the formation of alkanes (Equation 1) and that of alkenes (Equation 2) and it is traditionally performed starting from syngas (CO and H_2):

$$nCO + (2n + 1)\, H_2 \rightarrow C_2H_{2n+2} + n\, H_2O \quad (1)$$

$$n\, CO + 2n\, H_2 \rightarrow C_nH_{2n} + n\, H_2O \quad (2)$$

These reactions are highly exothermic and the temperature control during the process is a crucial parameter that significantly influences the final products formation and distribution [3].

Besides the operating conditions, the composition of the end products depends on the characteristics of the catalysts [4]. Cobalt-based catalysts have long been used for FT due to their long lifetime, high CO conversion and high selectivity towards heavy hydrocarbons [5]. Moreover, these catalysts exhibit low water-gas shift activity, which helps avoiding CO_2 formation. Ruthenium is commonly used in small amounts as an additive to promote cobalt reduction in supported catalysts [6].

In recent years, considerable progress has been made in the FT process. This includes new synthetic strategies for catalysts and the use of different raw materials to obtain fuels such as coal (CTL: coal to liquids), natural gas (GTL: gas to liquids) and biomass (BTL: biomass to liquids) [3]. Current research primarily focuses on improving the efficiency of heterogeneous catalysts and on increasing

58 the yield of the FT process. Also appealing is the prospect of using syngas with high CO_2 contents
59 (i.e. for BTL technologies) to produce carbon-neutral fuels [7]. However, the activation of the carbon
60 dioxide molecule is a challenge for the scientific community and the conversion and selectivity
61 reported so far are quite limited [8]. One approach to addressing this technological limit, consists in
62 developing new catalysts based on the same active metals as traditional ones (mainly Fe and Co) but
63 capable of achieving greater activity, higher conversion rate and better selectivity. In this regard, a
64 new class of promising catalysts are nano hydrotalcites (HTlc) [9].
65 HTlc are generally described by the formula $[M(II)_{1-x}M(III)_x(OH)_2]^{x+}[A^{n-}_{x/n}]^{x-}mH_2O$ where M(II) is
66 a divalent cation (Co, Mg, Zn, Ni, or Cu), M(III) is a trivalent cation (Al, Cr, Fe or Ga), A^{n-} is the
67 interlayer anion, and *m* is the molar amount of co-intercalated water.
68 To date, HTlc-based materials have been used as catalysts in various processes such as
69 transesterification, biodiesel production [10], steam reforming of ethanol for hydrogen production
70 [11], and methane reforming [12]. In recent literature, some studies have been carried out on Co-
71 based hydrotalcites [13], particularly in the use of HTlc as support of the FT catalyst [14] in which
72 the catalytically active metal is dispersed on HTlc surface [15]. HTlc are normally synthesized using
73 traditional methods, such as the co-precipitation or urea methods. Only recently, techniques like
74 ultrasonication and ball milling have been investigated for the preparation of HTlc used as catalysts
75 for CO_2 reduction by methanol synthesis or CO production. These synthetic methods have
76 substantially improved some characteristics of the catalysts promoting a higher dispersion of active
77 sites, particle size control and increased catalyst stability [16].
78 The ultrasound-assisted synthesis is an innovative green technique, which enables the creation of
79 materials with unique textural properties, a more uniform size distribution, higher surface area and
80 better-controlled phase composition [17, 18]. To ensure effective implementation of ultrasound-based
81 syntheses, it is crucial to regulate the emitted power in solution, frequency and sonication duration
82 [19]. Once these parameters are fine-tuned, the benefits are significant. One of the most noteworthy
83 is the improvement in catalytic performance due to a better distribution of the active phases on the

inert particles [17]. These improvements are promoted by the formation, growth and implosive collapse of bubbles induced by acoustic cavitation that create local extreme conditions (e.g., ca. 5000 °C and 1000 atm followed by cooling rates of more than of 109 Ks^{-1}) that prevent aggregation and crystallization of materials [20-22]. From an energy-saving perspective, the short synthesis duration (a few minutes) must also be considered. The use of ultrasound in the preparation of iron-based Fischer-Tropsch catalysts prepared by impregnation methodology was successfully evaluated in a previous work by observing an increase of the catalytic performance due to a better distribution of the active phases on the inert particle [17].

Another alternative emerging and sustainable method to prepare HTlc is the mechanochemistry. In this case, reactions are promoted by mechanical energy generated by a ball mill. This method enables the preparation of HTlc without solvents and with high yield, thereby minimising the environmental impact of the synthesis [23]. The short synthesis duration is another parameter to take into consideration when listing the benefits of this methods.

Ultimately, it has to be noted that both the techniques result in catalysts with a porous structure. Recent advancements in the field of microporous and mesoporous materials [24, 25] have shed light on the significant potential of such structures in catalysis. This is particularly relevant in the context of FT synthesis, where the pore structure of catalysts plays a critical role in determining their efficacy. The field of catalysis is continually evolving, with novel approaches emerging to enhance the efficiency of chemical processes. Recent advancements, such as the development of catalytic membranes for hydrocracking and hydro-isomerization [26], highlight the diversity and innovation in this field. In a previous work [27] a different kind of hydrotalcite, based on cobalt, was successfully tested for the syngas conversion. In alignment with this trend of catalytic innovation, the present study introduces a potential new kind of catalysts for the Fischer-Tropsch synthesis with particular interest in the application of CO_2 conversion, prepared with two innovative and energy-saving technologies as ultrasound-assisted co-precipitation and solvent-free mechanochemical synthesis.

The purpose of our study is to compare the effectiveness of ternary hydrotalcite-like compounds based on iron, copper and magnesium (MgCuFe), synthesized using the aforementioned methods: ultrasound-assisted co-precipitation and the solvent-free mechanochemical synthesis (ball milling). This novel approach aims to harness the unique properties of these materials for efficient CO_2 hydrogenation.

Activity tests, for CO e CO_2 hydrogenation, were conducted in a continuous packed bed reactor. SiO_2 was used as diluent [28, 29] since its presence improves both the activity, especially for Fe-based catalysts and the heat distribution in the reactor. The catalysts were analysed, both before and after the reaction, using FE-SEM-EDX, TEM, BET, TPR, XRD, TGA and (ATR) FT-IR analyses. This allowed us to establish correlations between the textural characteristics of the catalysts and their efficiency towards light and heavy hydrocarbons selectivity and to select the most promising method for synthesizing the best FT catalyst. The results of this research contribute to the growing body of knowledge in sustainable fuel production, showcasing the potential of nano hydrotalcite-based catalysts in environmental catalysis.

2. Experimental methods

2.1 Materials

Chemical reactants and catalysts precursors as $Mg(NO_3)_2 \cdot 6H_2O$, $Fe(NO_3)_3 \cdot 9H_2O$, $Cu(NO_3)_2 \cdot 3H_2O$, NaOH, $NaHCO_3$ and KNO_3 with analytical grade were purchased from Sigma Aldrich. All reagents were used as received without further purification. Reacting gases for FT synthesis were used directly from high purity (99.99%) cylinders purchased from Sapio Company.

2.2 Catalyst synthesis

Sample MgCuFe-US was synthesized by means of an ultrasound-assisted co-precipitation method. High power ultrasound irradiation was carried out by an Ultrasonic processors VC750 (Sonics and Materials) provided with a 13 mm diameter tip, operating at a 750 W, 20 kHz and 50 % of amplitude. The synthesis was carried out by adding 50 mL of 1M NaOH and 2M $NaHCO_3$ solution dropwise to 56 mL of 1M Mg, Fe, and Cu nitrate salts solution (molar ratio Mg/Fe/Cu=13.2/6/1). During the addition process, the solution was sonicated with ultrasound for 3.5 min, and the sample was maintained at 5°C. A yellow-brown solid immediately precipitated. At the end of the addition 100 mL of distilled water was added to suspend the precipitate. The solid was recovered by centrifugation and washed repeatedly with deionized water, then dried in an oven at 60°C in air. The final composition of MgCuFe-US, determined by ICP-OES (Table 1), is: $[Mg_{0.59}Cu_{0.07}Fe_{0.34}(OH)_2](CO_3)_{0.17}0.5\ H_2O$. MgCuFe-BM was synthesized with a solvent-free method by mixing the salts with a proper amount of NaOH pellets. To prepare 1 g of catalyst, 1.96 g of $Mg(NO_3)_2{\cdot}6H_2O$, 0.14 g of $Cu(NO_3)_2{\cdot}3H_2O$, 1.34 g of $Fe(NO_3)_3{\cdot}9H_2O$ and 0.888 g of NaOH (molar ratio Mg/NaOH = 3/1 molar ratio Mg/Fe/Cu=13.2/6/1) were ball milled for 30 minutes at a frequency of 30 Hz in a planetary mill (Retsch MM200 swing mill, capacity 10 mL, provided with agate balls with diameters 10 mm). The solid was collected and transferred in a PTFE bottle filled with 50 mL of distilled water. The precipitate was aged in an oven at 80°C for 3 days. The solid was recovered by centrifugation, washed three times with deionized water and dried at 60°C in air. The MgCuFe-BM composition, obtained by ICP-OES measurements (Table 1), is: $[Mg_{0.62}Cu_{0.06}Fe_{0.32}(OH)_2](CO_3)_{0.16}\ 0.5\ H_2O$.

Table 1. Experimental weight ppm of Mg, Cu and Fe as determined by ICP and the corresponding molar fractions of the fresh and spent catalysts

sample	Mg (ppm)	Cu (ppm)	Fe (ppm)	x_{Mg}	x_{Cu}	x_{Fe}
MgCuFe-US **fresh**	8.79	2.73	11.70	0.59	0.07	0.34
MgCuFe-BM **fresh**	8.95	2.09	10.78	0.62	0.06	0.32
MgCuFe-US **spent**	4.46	1.42	5.92	0.59	0.07	0.34
MgCuFe-BM **spent**	6.30	1.71	7.79	0.61	0.06	0.33

Before the catalytic tests the samples were impregnated with KNO_3. In detail, MgCuFe-US and MgCuFe-BM were soaked for 2 h in a KNO_3 solution (K = 0.5 wt%) at T= 60°C. The samples were dried at 80°C until all water was removed.

2.3 Characterization of Catalysts

The specific surface area (SBET) and porosity distribution were obtained from N_2 adsorption/desorption isotherms at 77 K using a Tristar II 3020 (Micromeritics) apparatus and the instrumental software (Version 1.03) and applying Brunauer–Emmett–Teller (BET) and Barrett–Joyner–Halenda analyses, respectively. Prior to measuring, sample powders were thermally pre-treated (T = 150 °C, 4 h, N_2) to remove adsorbed species such as water.

X-ray powder diffraction (XRPD) patterns were collected with a Bruker D8 Advance diffractometer (Bruker AXS GmbH, Karlsruhe, Germany) equipped with a Lynxeye XE-T fast detector and CuKa radiation. The operative conditions were 40 kV and 40 mA, with a step size of 0.033° 2θ and a step scan time of 30 s. Phase identification was performed using the Bruker DIFFRAC.EVA V5 software, and a COD database. Quantitative analyses of crystalline phases have been performed applying the Rietveld method with the help of the Bruker AXS Topas Version 6 software.

The metal content of the samples, before and after the catalytic tests, was determined by inductively coupled plasma optical emission spectrometry (ICP-OES), using a Varian Liberty Series instrument. Thermogravimetric analyses (TGA) were obtained using a Netzsch STA 490 C TG-DTA thermal analyzer, operating at 10 °C/min heating rate and 30 mL/min air flow.

Attenuated total reflection (ATR) FT-IR measurements were carried out using a Shimadzu IR-8000 spectrophotometer. The spectral range measured was 400 to 4000 cm^{-1}, with a spectral resolution of 4 cm^{-1} acquiring 100 scans.

The morphology and composition were examined by Field Emission Gun Electron Scanning Microscopy (FE-SEM) LEO 1525 ZEISS. Elemental composition and chemical mapping were determined using a Bruker Quantax EDS.

TEM images were obtained using a Philips 208 Transmission Electron Microscope. The samples were prepared by placing a drop of an ethanol dispersion of the catalyst powder on a copper grid pre-coated with a Formvar film and air-dried.

Contact angle measurements were performed using water as the medium. The instrument is a Data Physics OCA 150 equipped with a SCA20 version 2.3.9 build 46 software. The analysis was performed to check the hydrophilicity of the two catalysts, both as fresh and after performing the activation. The reported results were determined as average of four measurements.

The Temperature Programmed Reduction (TPR) measurements were carried out by placing the catalyst (25 mg) in a quartz reactor heating in a reductive mixture flow (5% H_2/Ar) at a heating rate of 10 °C/min from 25 to 1000 °C. Hydrogen consumption was monitored by a TCD detector with a W/Re filament in the Autosorb IQ instrument.

Temperature programmed desorption using CO_2 as a probe molecule (CO_2-TPD) was carried out in a lab-made equipment. Samples (25 mg), previously cleaned in He flow (30 mL/min) at 110 ° C for 0,5 h, were inserted in a quart reactor. After cooling to 40 °C, the samples were exposed to CO_2 pulses of 0.44 mL each to achieve over saturation. After cleaning the surface with He flow (30 mL/min) for 0.5 h at 40 °C, samples were heated with a temperature rate of 10 °C/min from 40 °C to 1000 °C in He flow (30 mL/min). Gases were monitored by a Gow-Mac TCD detector with a AuW_2 filament.

2.4 Catalytic test

During FT reaction (H_2/CO as reactants) Brooks mass flow controllers were used to measure the amount of H_2 (32 Nml min^{-1}, 99.99% purity), CO (16 Nml min^{-1}, 99.99% purity), and N_2 (internal standard, 5 Nml min^{-1}, 99.99% purity) in a continuous mixer. In the case of carbon dioxide hydrogenation reaction, the H_2/CO_2 ratio was set to 3, with the flow of reactants being 36 Nml min^{-1}, 12 Nml min^{-1}, and 5 Nml min^{-1}, for H_2 (99.99% purity), CO_2 (99.99% purity) and N_2 (99.99% purity) respectively.

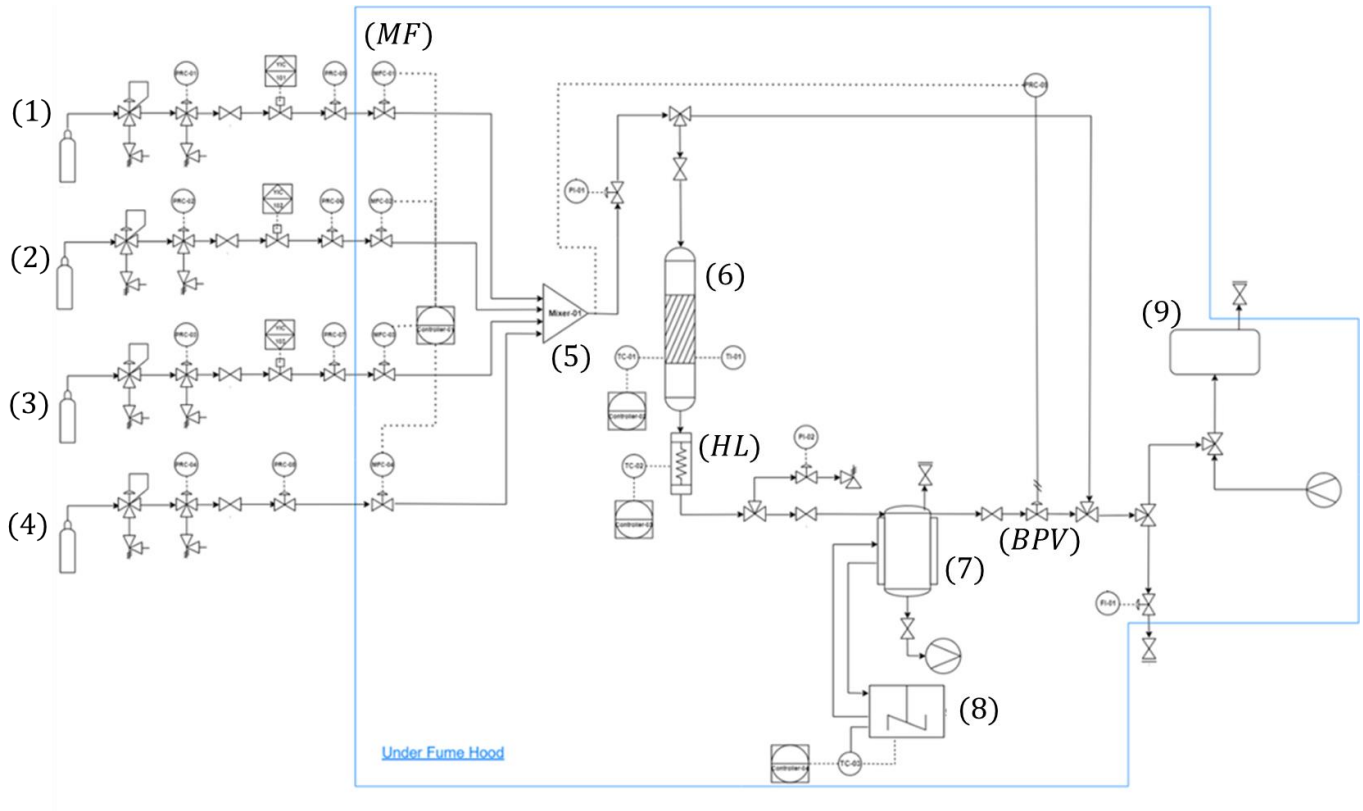

Fig. 1: Laboratory scale plant used for catalytic tests. (1) CO cylinder, (2) H_2 cylinder, (3) N_2 cylinder, (4) CO_2 cylinder, (MF) Mass flowmeters, (5) Mixing chamber, (6) Reactor, (HL) Hot line, (7) Cooling trap, (8) Refrigerator, (BPV) Back pressure valve, (9) In-line Micro-GC analyzer.

The reactor used in the experiment had a 6 mm internal diameter and was packed with 1 g of new catalyst and 0.5 g of SiO_2 as diluent to improve the heat loss [24, 25].

To prevent any false results, a blank test was conducted to ensure that the inner surfaces of the plant were inactive. The catalyst was held in place by a quartz wool bed divided into two separate sections. The reactor was heated with a furnace and the temperature was measured using a K-type thermocouple. A second K-type thermocouple monitored the reactor temperature.

To activate the catalyst, a 2/1 molar ratio of H_2/CO mixture (53 Nml min^{-1}) was flowed in the reactor for four hours at 350 °C and 0.4 MPa. At 5 °C, liquid products such as water and C_{7+} (i.e., liquid hydrocarbons having more than 7 carbon atoms) were condensed in a 0.13 L cold trap with an external cooling jacket before being examined by gas chromatography.

To maintain a pressure of 2.0 MPa, a pneumatic back pressure regulator was utilized [27, 30, 31]. Permanent gases and non-condensable hydrocarbons went through another condenser and were examined by an Agilent 3000A micro gas chromatograph to calculate CO and CO_2 conversion (X_{CO2} and X_{CO}). This was based on the peak areas of N_2 and CO_2/CO peak areas (A_{N_2}, A_{CO} and A_{CO_2}), their relative response factor (k), and input (set) flow rate of N_2, CO and CO_2 (F_{in,N_2}, $F_{in,CO}$ and F_{in,CO_2}) (Eq.3 and 4).

$$X_{CO2} = \frac{F_{in,CO2} - F_{in,N_2}}{F_{in,CO2}} \times k \frac{A_{CO2}}{A_{N_2}} \quad (3)$$

$$X_{CO} = \frac{F_{in,CO} - F_{in,N_2}}{F_{in,CO}} \times k \frac{A_{CO}}{A_{N_2}} \quad (4)$$

The oxygenated compounds produced during FT test were assumed to have completely solubilized in the water phase collected in the cold trap. The analysis of this liquid was carried out using a Shimadzu 5000 A Total Organic Carbon instrument.

To ensure accurate measurement of gas compositions during the Fischer-Tropsch tests, a calibration procedure was employed using pure cylinders of CO_2, CO, and H_2. The flow rates of these gases were set by Brooks mass flow controllers and then quantified with a micro-GC analyzer. This calibration was crucial for establishing reliable baseline data for the accurate quantification of reactants and products in the FT tests.

The FT tests with syngas (CO/H_2 mixtures) were performed at temperatures ranging from 200-300C°. More in detail, the furnace temperature was first increased to 200 °C and held for about 18 hours. Then, it was raised to 220 °C and maintained for 24 hours before repeating the process for 250 °C, 270°C, 300°C. Similarly, for the CO_2/H_2 starting feed, the same catalysts were tested at temperatures of 275, 310, 350°C, and at a pressure of 20 bar. The same procedure described above was followed, except for the feed molar ratio CO_2/H_2 of 1:3 instead of CO/H_2 of 1:2.

3. Results and discussion

3.1 Characterization

SEM and TEM images of the MgCuFe-US and MgCuFe-BM samples are shown in Figure 2. In both cases, the crystals appear approximately flat and hexagonal, but the platelet size distribution is not uniform. The samples consist of platelets ranging from 30 to 150 nm, with a greater proportion of small crystals in MgCuFe-US. The synthesis method also affects the crystallinity, which is lower in the ball-milled sample.

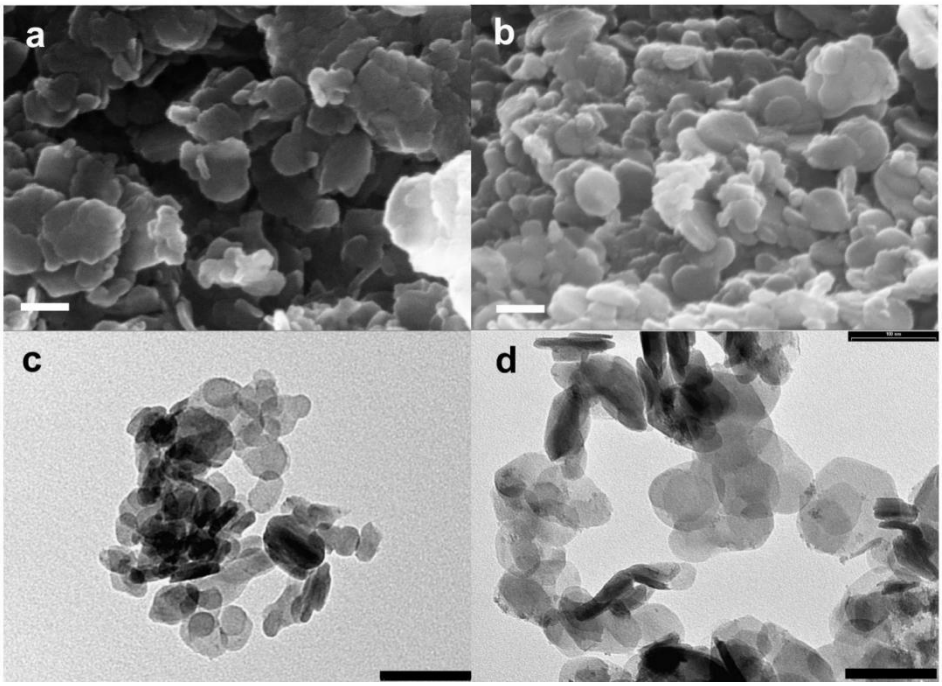

Fig. 2: SEM and TEM images of MgCuFe-US (a and c) and MgCuFe-BM (b and d). The scale bars indicate 100 nm.

An indication of the different degree of crystallinity is evidenced by comparing the XRD patterns of the samples, shown in Figure 3. Both samples are characterized by typical hydrotalcite-like compound patterns at 11.6°, 23.3°, 34.3°, 59.6°, and 61.0°, which correspond to *(003)*, *(006)*, *(012)*, *(110)*, and *(013)* crystallographic planes [32]. The interlayer space of HTlc hosts carbonate ions, as evidenced

by the position of the first reflection at 2θ = 11.6°. The XRD patterns of MgCuFe-BM before and after the thermal treatment suggests that the as-synthesised sample is mostly amorphous, as the peaks are broad and the *(110)* and *(013)* diffraction planes are not clearly distinguished, appearing as a single reflection. Even after the aging process, the reflections of MgCuFe-BM have a larger full width at half maximum than those of MgCuFe-US, indicating the presence of crystallites with smaller size.

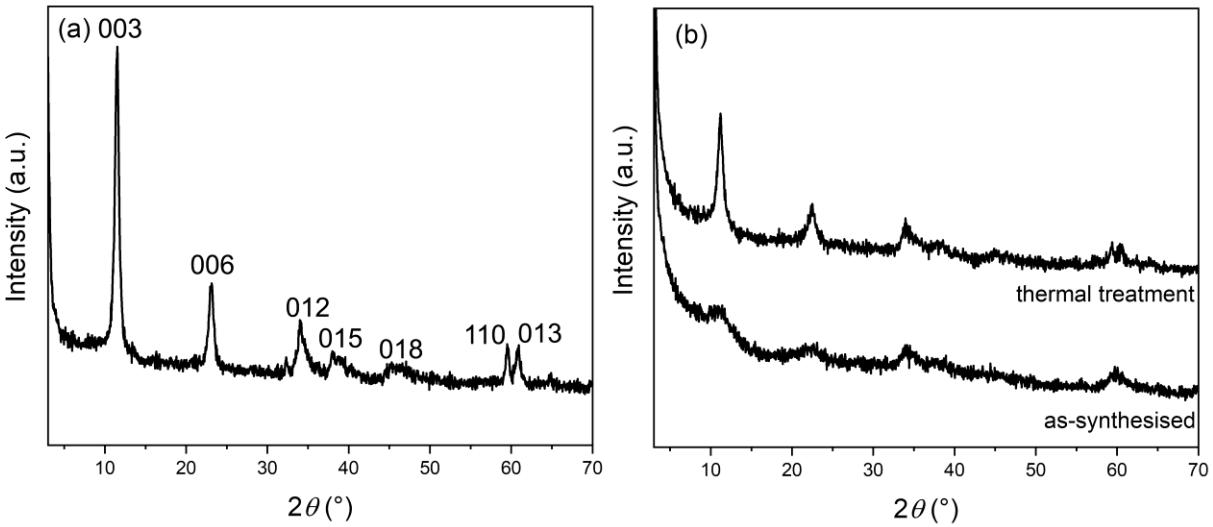

Fig. 3: XRD of as synthetised MgCuFe-US (a) and MgCuFe-BM (b).

The samples were characterized by TGA in order to study their thermal decomposition (Fig. 1 SM). The ATR FT-IR spectra confirmed the formation of HTlc in carbonate form (Fig. 2 SM).

After the impregnation with K, the samples were activated by CO/H_2 and analysed by XRD patterns (Figure 4). A quantitative analysis of the phases was also performed (Table 1 SM, Figure 3 SM).

Figure 4 shows the XRD patterns of the samples that were activated by CO/H_2 before undergoing the catalytic FT test. This activation procedure involved feeding CO/H_2 syngas mixture at 350°C and 0.4 MPa for 4 hours directly in the catalytic reactor. Both diffractograms depict the presence of $MgCO_3$. This phase is formed due to CO_2 activation on the surface of the basic oxide, MgO, which leads to the formation of the carbonate [33]. Additionally, the activating conditions (350 °C and 0.4 MPa), resulted in the detection of Fe_2C_5 (double peak at 2θ= 43.4° and 44.1°), presumably the active species in the FT process, along with superimposed phases of iron-based spinels such as Fe_3O_4 [34].

Moreover, especially in ultrasound-prepared samples, the presence of $Na_2Mg(CO_3)_2$ is evident. This may derive from the trace amount of sodium derivatives already contained in the synthesized samples. The morphology of the samples was investigated using SEM and TEM after CO/H_2 syngas activation. Figure 5 shows the images obtained from the analysis, which reveal that the crystals maintained a flat morphology in all cases. The presence of iron carbide species, as revealed by XRD, is somewhat confirmed by TEM analysis. The TEM images also hint at the presence of a non-specified carbide [35]. This was indicated by the covering layer formed on the surface of the crystals after the activation, as seen in Figures 5c and 5d. This difference is evident when comparing the TEM images of the samples.

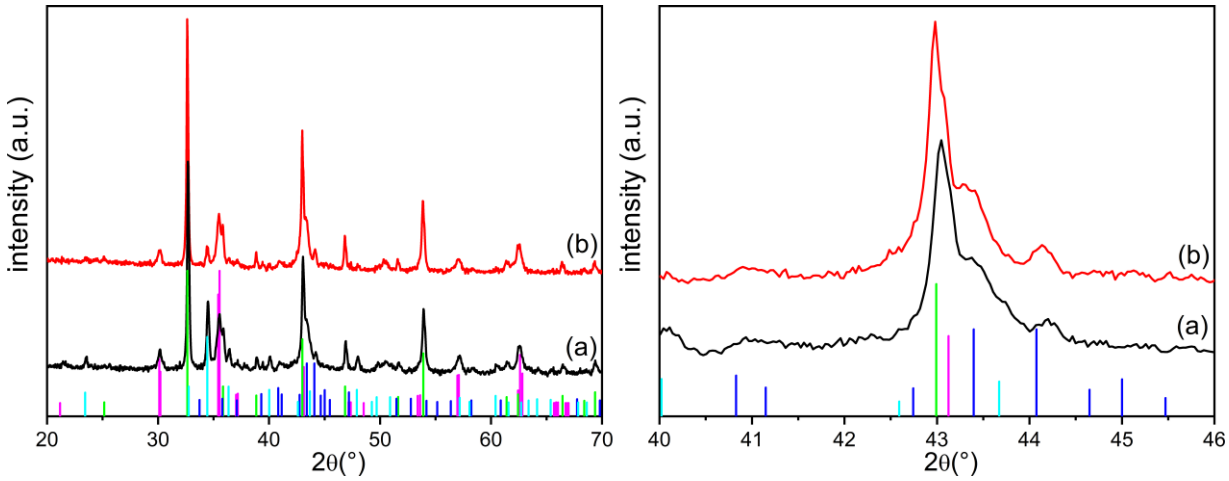

Fig. 4: XRD patterns of activated catalysts with Syngas at 350°C: (a) MgCuFe-US and (b) MgCuFe-BM (left). Enlargement in the 40-46 2theta range (right). Fe_3O_4 (magenta line, COD#1532796) and/or $MgFe_2O_4$ (magenta line, COD#1011241), $MgCO_3$ (green line, COD#2101057), Fe_2C_5 (blue line, COD#1521831), $Na_2Mg(CO_3)_2$ (cyan line, COD#9000298).

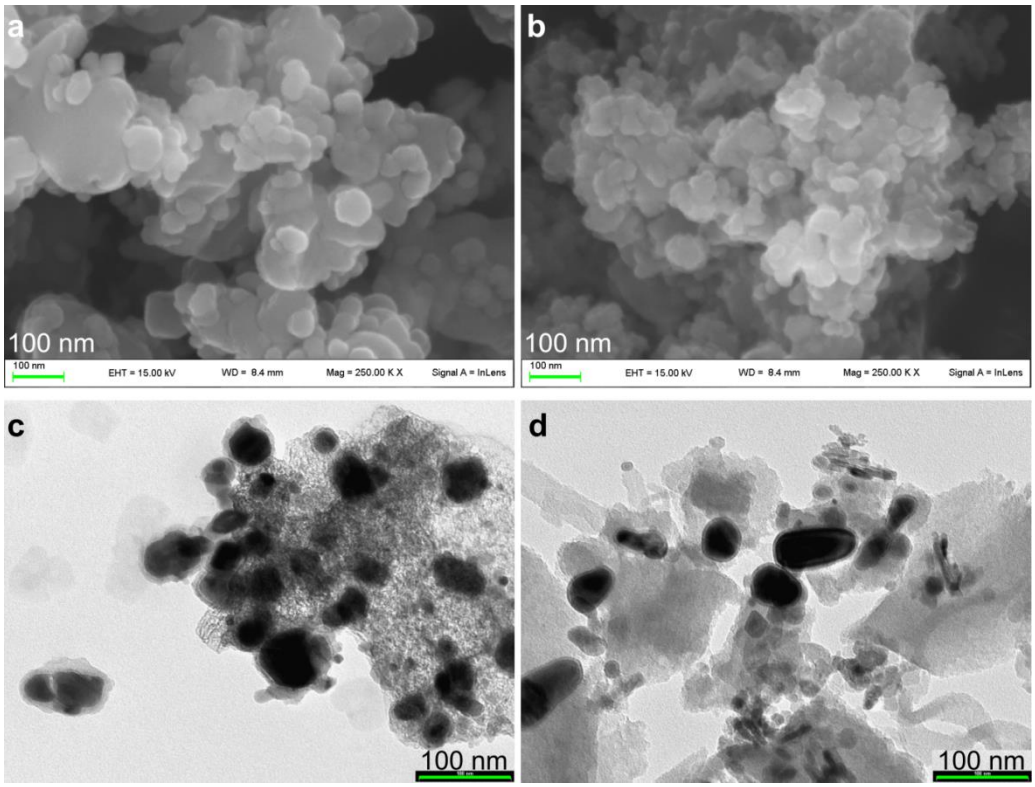

Fig. 5: SEM and TEM images of MgCuFe-US (a and c) and MgCuFe-BM (b and d) activated with syngas.

Table 2: Specific surface areas

Catalyst	BET surface area (m^2/g)	volume of pores (cm^3/g)
MgCuFe-US fresh	87	0.34
MgCuFe-US activated	31	0.23
MgCuFe-BM fresh	112	0.30
MgCuFe-BM activated	41	0.19

The specific surface area and pore structure of catalysts play a crucial role in determining their catalytic efficiency, especially in processes like Fischer-Tropsch synthesis. In our study, we measured the BET surface area of the freshly synthesized MgCuFe-BM and MgCuFe-US catalysts, and found them to be 112 m^2/g and 87 m^2/g, respectively (Table 2). These values are in accordance with those typically observed for hydrotalcite-like compounds [36, 37]. According to IUPAC classification, their isotherms are of type IV (Figure 6) (Table 2) with an H3 hysteresis loop, indicating a mesoporous structure [38]. With non-rigid aggregates of plate-like particles, in agreement with SEM results. This structure favors mass transport of reactants and products within the catalyst.

Upon activation, a decrease in surface area and cumulative pore volume was observed for both catalysts (MgCuFe-US values: 31 m^2/g and 0.23 cm^3/g, and MgCuFe-BM to 41 m^2/g and 0.19 cm^3/g). This decrease is likely due to structural changes that occur at high temperatures, particularly close to the activation temperature of 350 °C. These changes cause the collapse of smaller pores, leading to an increase in the average pore width and a decrease in total pore volume. As a result, activation step potentially affects the accessibility of reactant molecules to active sites, ultimately impacting the reaction rate. Nevertheless, both MgCuFe-US and MgCuFe-BM retained their mesoporous structure, as demonstrated by the adsorption isotherms performed on fresh and activated samples (Figure 6).

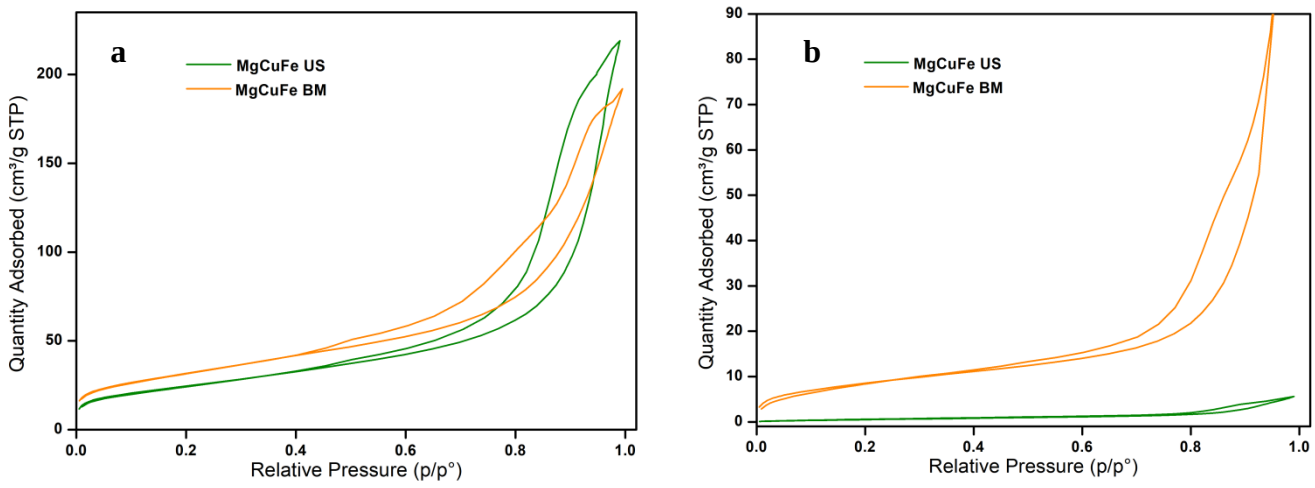

Fig. 6: BET adsorption isotherms a) before the catalytic test, fresh catalyst and b) after activation.

These results are in accordance with literature data reporting that sonochemical synthesis typically results in finer, loosely agglomerated particles with larger pores [39, 40], whereas mechanochemical synthesis often leads to denser, more tightly packed agglomerates with smaller pores. The implications of these findings are significant for the catalytic performance of MgCuFe-US and MgCuFe-BM, suggesting that, depending on the desired reaction and on the size of the reactants, it is possible to tune the most effective structure by changing the synthesis method.

These results are confirmed by pore size distribution (Table 3), which reveals a difference between the two hydrotalcites and the two synthesis methods. In particular, the as- synthesized ball milled sample contains smaller pores compared to the fresh ultrasound sample, which is constituted by larger pores. This trend is maintained even after the activation. As reported above, such structural differences affect the diffusion of reactant/product molecules, and hence the reaction rate and yield. The largest pores in MgCuFe-US allow easier diffusion and retro-diffusion from catalytic sites, potentially enhancing the reaction rate for larger molecule reactants. Conversely, the smallest pores in MgCuFe-BM could be more effective for reactions involving smaller molecules, as they offer a higher surface area per unit volume, increasing the likelihood of reactant-catalyst interactions. SEM and TEM analysis support this finding, showing that ultrasonic synthesis tends to produce smaller particles and larger pores compared to ball milling.

Table 3: pore size distribution of the fresh catalysts (as %) in nm

Catalyst	2<d<5	5<d<10	10<d<20	20<d<50	50<d<100	100<d
MgCuFe-US fresh	42.0	16.9	16.6	17.1	6.8	0.5
MgCuFe-US activated	23.8	14.3	30.8	21.2	5.1	4.7
MgCuFe-BM fresh	53.9	18.7	16.2	9.3	1.4	0.5
MgCuFe-BM activated	58.8	16.7	18.0	5.4	1.0	0

In FT-CO_2 hydrogenation, water is a byproduct. The hydrophobic nature of catalysts is crucial for efficient operation [41]. Contact angle measurements for the MgCuFe nano hydrotalcites catalysts reveal essential insights. The fresh MgCuFe-US catalyst has a contact angle of 75.81°, indicating moderate hydrophilicity. However, after activation, this angle decreases to 57.92°, suggesting increased hydrophilicity, which might be less desirable in CO_2 hydrogenation due to potential challenges in water removal.

In contrast, the fresh MgCuFe-BM catalyst starts at a hydrophilic 59.92°, but after activation, it shifts to a slightly more hydrophobic angle of 62.65°. This subtle increase in hydrophobicity could be advantageous for CO_2 hydrogenation, as it implies better water management, maintaining catalyst efficiency and preventing deactivation.

Overall, the observed changes in contact angles indicate the significant impact of synthesis and activation methods on the catalysts' surface properties. While initial hydrophilicity might offer some benefits, a trend towards hydrophobicity, particularly after activation, aligns more effectively with the needs of CO_2 hydrogenation. These insights highlight the importance of tailoring surface properties, prioritizing hydrophobic characteristics to optimize performance in reactions where efficient water management is crucial.

3.2 FT Activity test

The main products of the Fischer-Tropsch reaction are CH_4, CO_2, H_2O and C_xH_y in the range of C_1 to C_{100}. The distribution of C_xH_y follows the so-called Anderson-Schulz-Flory distribution (Eq. n°5). According to this theory, the mass distribution (w) depends on two factors: the number of monomer units (k) and an empirical factor, the α value which is a number from 0 to 1:

$$w_n\,(n) = \alpha^{n-1} n (1-\alpha)^2 \quad (5)$$

From Eq. 5 it is possible to obtain a linear relationship (Eq. 6) between the carbon number of a product and its relative weight fraction.

$$\ln\left(\frac{w_n}{n}\right) = \ln(1-\alpha)^2 + (n-1)\cdot \ln \alpha \quad (6)$$

The length of the hydrocarbon chain depends on the chain growth probability (α), which can be determined by analysing the semilogarithmic graphs and it defines the products obtained. The higher the α, the longer the hydrocarbons chains.

MgCuFe-BM and MgCuFe-US catalysts were tested both for classical FT reaction (CO and H_2 as feed) and CO_2 hydrogenation (CO_2 and H_2 as feed) for the production of hydrocarbons. The results will be presented based on CO and CO_2 conversion rates, as well as the selectivity towards methane, carbon dioxide, light hydrocarbons (C_{2-6}), and heavy hydrocarbons (C_{7+}). The total yield to C_{2+} hydrocarbons is calculated by combining the results of both conversions and product selectivity as calculated by Equations (7) and (8). Methane and carbon dioxide will not be considered in the total yield calculation since they are usually regarded as undesired products in the FT process.

C_{2+} *total yield = CO conversion X (selectivity* $<C_7$ *+ selectivity* $>C_7$*) x* 10^{-2} (7)

C_{2+} *total yield =* CO_2 *conversion X (selectivity* $<C_7$ *+ selectivity* $>C_7$*) x* 10^{-2} (8)

All the data presented in this paper pertains only to the steady state conditions of the experimental plant. It took 14 hours for the FT reactor to reach this state, during which the flow rate and composition remained constant with respect to reaction time. Therefore, we only provide data collected after this initialization period.

It is important to note that the activation step directly performed in the reactor before starting the FT test, strongly influences the catalyst's performance.

In particular, it is well-known that iron carbide, a highly active species in FT, can be formed by using a mixture of H_2 and CO for activation [42]. To investigate this, we performed TPR and CO_2-TPD analyses on these catalysts activated by pure H_2 or H_2/CO mixture and found no significant differences in the results (see Fig. 4-5 SM), these analyses were discussed in the Supporting Materials. Based on these findings, all the catalysts used in this paper, were activated by means of a flowing mixture of H_2/CO in the reactor.

Regarding conversions obtained, Figures 8 and 9 illustrate the ultrasound and ball milled catalysts used in the study.

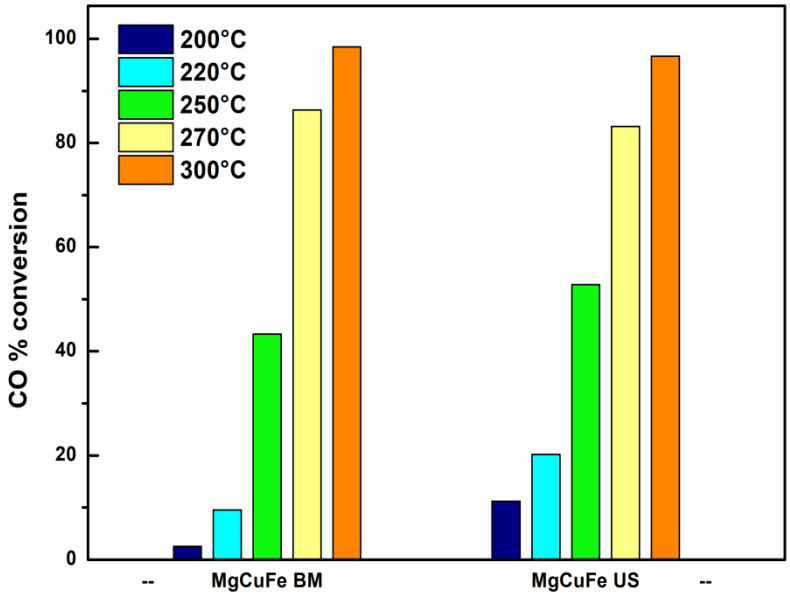

417 **Fig. 7**: CO conversions at different temperatures using MgCuFe-BM and MgCuFe-US catalysts.

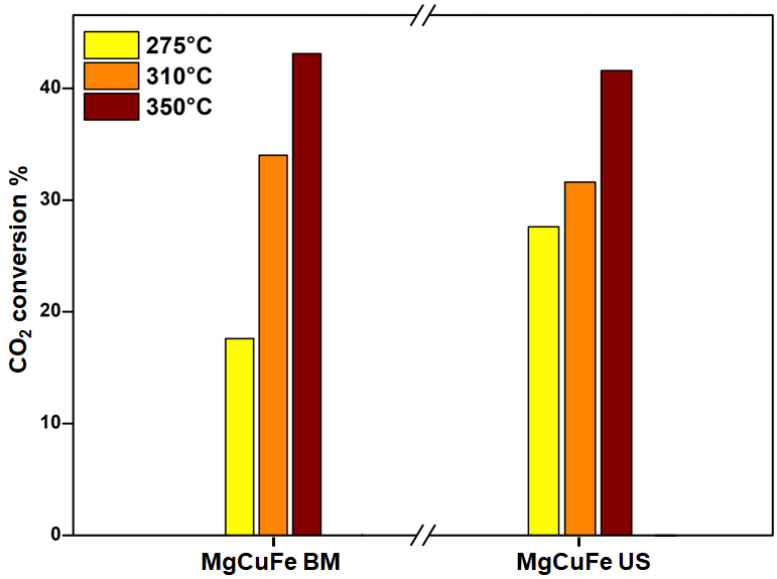

418

419 **Fig. 8**: CO_2 conversions at different temperatures using MgCuFe-BM and MgCuFe-US catalysts.

420

421

422

423

424

425

Table 4: C_{2+} yields

Mixture feed	Temperature °C	MgCuFe-US	MgCuFe-BM
		C_{2+} yield	
CO_2/H_2 (1:3 molar ratio)	275	21.2	11.7
	310	22.3	25.8
	350	34.1	35.8
CO/H_2 (1:2 molar ratio)	200	8.7	1.8
	220	12.9	6.4
	250	28.5	24.7
	270	45.3	49.2
	300	51.3	50.2

Results of TOC analyses showed that oxygenated compounds had a very low concentration (<0.5%) in all the catalytic tests. GC-Mass analysis of the condensed phases corroborated the TOC results, confirming that the alcohol content was below 0.5% by weight. The catalysts containing integrated iron in the HTlc structure were proven to be highly active for CO and CO_2 hydrogenation in FT synthesis, as demonstrated by the satisfactory results presented in Table 4 and Figures 8 and 9. This is not commonly observed in other studies in the literature [43], where iron is mostly utilized in its metallic form in Fe-supported catalysts.

By feeding CO/H_2 mixtures, increasing the reactor temperature, the activity of both catalysts increases, as expected, leading to higher CO conversion and greater selectivity towards CO_2, CH_4, and light hydrocarbons. In particular, CH_4 percentage swings from 1-2% up to 6% while CO_2 starts

at 20% at 200°C increasing gradually to ca 40% at 300°C. The maximum conversion is observed for both MgCuFe-US and MgCuFe-BM at 300 °C (Fig 8), with difference in activity detected at lower temperatures. In fact, at temperatures ranging from 200 to 250 °C, the MgCuFe-US sample exhibits a CO conversion rate roughly 10% higher than that of the MgCuFe-BM sample. The same phenomenon is observed during CO_2 hydrogenation reaction with US reaching ca. 20% increase in CO_2 conversion at 275 °C.

Significant variation is observed in terms of lighter hydrocarbon cut (C_{2-6}) and heavier one (C_{7+} fractions). As the temperature increases, the MgCuFe-BM sample has a higher C_{2-6} yield than the MgCuFe-US sample, while the latter exhibits a higher selectivity towards C_{7+} hydrocarbons [44]. This can be explained considering that the MgCuFe-BM sample showed a higher concentration of lower pore size particles both in fresh and activated form, while the ultrasound sample displayed greater predominance of larger pore size particles, thus yielding longer hydrocarbon chains as products. The correlation between catalysts pore size and catalytic activity has been investigated in literature and is line with the above-mentioned results [45]. The fact that the total C_{2+} yield has comparable values demonstrates that, even if the conversions are almost equal, the selectivity towards short and long hydrocarbon chains is proven to be distinct between the two-iron based hydrotalcites. In the case of CO_2/H_2 as feed, similar trends were observed (Table 5), with the MgCuFe-US catalysts still showing higher selectivity for C_{7+} hydrocarbons in all evaluated temperatures, while the MgCuFe-BM catalysts showed higher selectivity for C_{2-6} hydrocarbons. The selectivity to methane and carbon monoxide remained stable and under 20% for the CO and 12% for methane.

Table 5: Hydrocarbon selectivities with starting feed CO_2/H_2

Temperature °C	**MgCuFe-BM**		**MgCuFe-US**	
	%C2-6	%C7+	%C2-6	%C7+
275	33.9	32.8	37.3	42.5
310	42.4	33.5	34.5	36.2
350	51.9	31.2	48.6	33.4

The differences in selectivity are confirmed through the evaluation of the hydrocarbon distribution (α) obtained from the cooled trap by GC analysis of the heavier cut.

When working with CO/H_2 as initial feed, α values are substantially different between the two catalysts, being 0.86 for the MgCuFe-US and 0.79 for the MgCuFe-BM.

The same phenomenon was investigated for the tests performed after the CO_2 hydrogenation (Fig 9). In the case of MgCuFe-US sample, the α value of 0.62 is significantly higher than 0.51 which was obtained using the MgCuFe-BM catalyst.

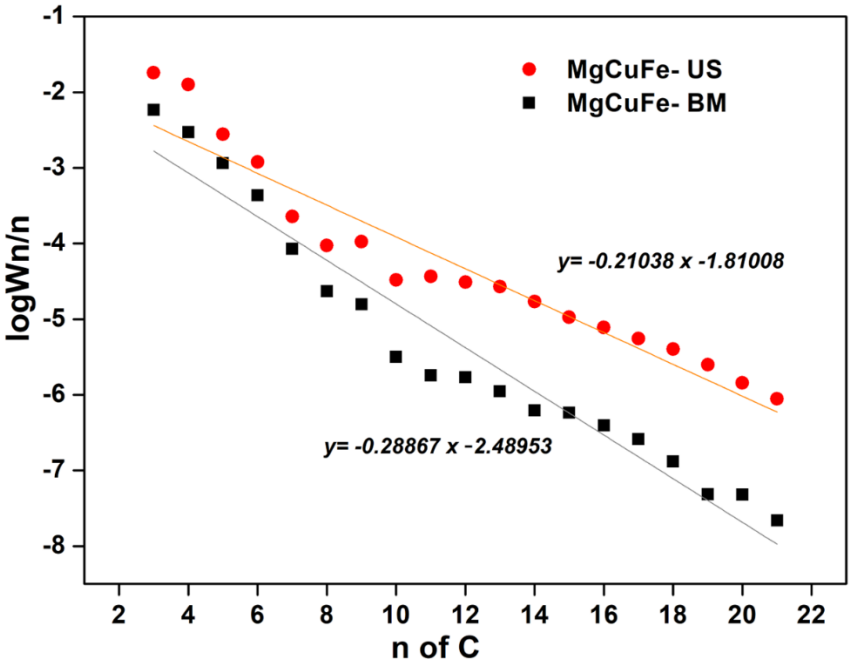

.

Fig. 9: Chain propagation probability α, at 310°C and CO_2/H_2 feed.

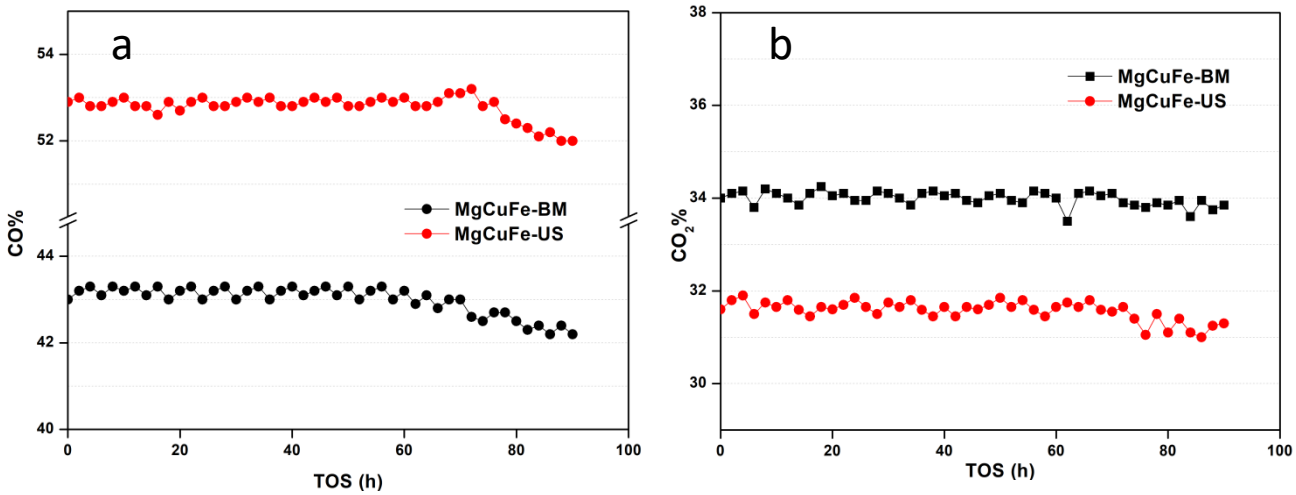

Fig. 10: Catalytic stability of the two samples with different feeding mixtures, TOS = time on stream, a) isotherm catalytic test at 250 °C, CO% =carbon monoxide conversion. b) isotherm catalytic test at 310°C, CO_2% =carbon dioxide conversion.

Taking into consideration the composition of activated catalysts and the results of surface area and contact angle, we can make assumptions about how the surface of the catalyst interacts with the substrate and explain its reactivity. During the activation phase, the catalyst is heated for four hours in the reactor. The heat causes HTlc to dehydrate and to progressively dehydroxylate. As a consequence, the HTlc structure partially collapses, making the basic sites composed of M-OH (M=Mg, Fe, Cu) more accessible to the syngas as confirmed by CO_2-TPD (Fig. 5 SM). As the temperature increases, HTlc converts to mixed oxides that act as Lewis acid-basic pairs and interact with syngas starting the synthesis [46]. Among the oxides, Fe_3O_4 is responsible for the reverse water-gas shift (RWGS) reaction, which is crucial in the reduction step of CO_2 to CO in the CO_2-FT reaction. As indicated by the XRD patterns in Figure 4, another product of HTlc activation is Fe_2C_5, which drives the subsequent hydrogenation of CO through the classical FT reaction [47]. The RWGS step is endothermic, meaning it is favored at higher temperatures. This is demonstrated by the increased conversion rate at correspondingly increased activation temperature.

The different yields at lower temperatures can be explained based on the degree of aggregation and surface roughness of the two HTlcs. These parameters influence the contact angles. HTlcs produced through ball milling have a more disordered structure and agglomerated particles. This results in a denser product with less interparticle space, which leads to reduced water permeability and hydrophilicity. On the other hand, the sample prepared through ultrasonication has a more crystalline structure and larger spaces between particles, which improves wettability. Upon activation, the disparity in value between the two contact angles reduces significantly (from 15.89° to 4.73°) as compared to the fresh samples. Additionally, the yields obtained from both samples are almost

identical. This indicates that activation process partially eliminates the initial differences that were caused by the distinct synthesis methods.

Together with the morphological stability revealed by XRD analysis, an activity evaluation was also performed. Considering the two experiments, performed at different temperatures, as reference cases, a 90-hour catalytic run was performed to assess the stability of CO and CO_2 conversion over time. As evidenced by Figure 10, the conversions remain consistent throughout the TOS, with negligible discrepancies of less than 1% for both samples. This suggests satisfactory stability in the catalytic activity over prolonged use, whether CO or CO_2 is used as a starting reagent. Moreover, the composition of the catalysts recovered after the reaction was analysed via ICP-OES, and it was found that there was no change in comparison to the pristine samples (the molar fractions vary by maximum 3%, Table 1). The active phases (Fe_5C_2 and Fe_3O_4) are still present in the spent compounds as evinced by the phase analysis (Table 2 SM and Figure 6 SM). In addition, metallic Fe and Cu were detected only in MgCuFe-US, graphite in MgCuFe-BM while $FeCO_3$ is common in both the samples and $Na_2Mg(CO_3)_2$ disappears.

Studies on other iron-based compounds were compared with the investigated hydrotalcite performance, revealing that the catalyst exhibited a higher catalytic activity than classical silica-supported iron catalysts like FeSi or FeSBA-15 [42], but slightly lower performance than the expensive iron-based metallosilicates like $Fe/Ce/SiO_2$ and $Fe/Zr/SiO_2$ [26, 48-51]. For instance, at 280 °C and 1.5 MPa, the Fe15Si catalyst achieved 50% CO conversion, with a heavy hydrocarbon cut selectivity below 40% [48-50, 52]. This comparison highlights the enhanced efficacy of our catalysts, especially in achieving higher conversion rates and balanced selectivity towards heavier hydrocarbons under similar reaction conditions. On the other hand, the previously mentioned metallosilicates exhibit CO conversion ranges between 50 and 60% at 250°C and 2.0 MPa, with heavy phase selectivity between 55 and 65% [46]. This comparison indicates that while our hydrotalcite-based catalysts surpass traditional iron-based catalysts in terms of activity, there is still room for optimization to reach the efficiency levels of the latest metallosilicates.

The performance of our MgCuFe US and MgCuFe BM catalysts was also compared with various iron-based catalysts reported in the literature for CO_2 hydrogenation. As benchmark for the comparison, results achieved at 310°C, 20 bar, and a GHSV of 3200 ml $gcat^{-1}$ h^{-1} were considered. The MgCuFe BM catalyst exhibited a CO_2 conversion of 34.4% and a C_{2+} selectivity of 75.9%, while the MgCuFe US catalyst showed a CO_2 conversion of 31.9% and a C_{2+} selectivity of 70.7%. Comparatively, the 92.6Fe7.4K catalyst [53] achieved a CO_2 conversion of 41.7% and a C_{2+} selectivity of 83.8%, and the 10Fe0.8K0.53Co catalyst [54]] showed higher CO_2 conversion of 54.6% with a selectivity of 79.1%. Both were tested at 300°C and 25 bar with a GHSV of 560 ml $gcat^{-1}$ h^{-1}. The K-Fe15 catalyst [55], at 300°C and 10 bar, reported a CO_2 conversion of 48.5% and a selectivity of 74.4%.

Other catalysts, such as the 1wt% Na-10 wt % Fe/ZrO_2 [56], showed lower selectivity (46.6%) and similar conversion (39%) at 340°C and 20 bar, while the 10Fe3Zn1K/Al_2O_3 [57] had a CO_2 conversion of 38.6% but much lower selectivity (30.9%) at 400°C and 30 bar.

The $CuFeO_2$-12 catalyst [7] had a lower CO_2 conversion (18.1%) and selectivity (65.4%) compared to our catalysts. Similarly, the 5Na/Fe catalyst [56] at 340°C and 20 bar showed lower conversion (24%) and selectivity (47.3%).

The 20Fe-1K/m-ZrO_2 catalyst [58] and $ZnFeO_x$-4.25Na catalyst [59] also demonstrated lower performance in terms of selectivity compared to our catalysts, with 30% and 75.2% C_{2+} selectivity, respectively.

Overall, our MgCuFe BM and MgCuFe US catalysts show competitive CO_2 conversion rates and high selectivity towards C_{2+} hydrocarbons, outperforming several reported catalysts, particularly in terms of selectivity. This demonstrates the effectiveness of our synthesis methods and the potential of these catalysts for CO_2 hydrogenation applications and opens the possibility to evaluate with interest the application of these materials, scarcely investigated till now for the Fischer Tropsch synthesis, for CO and CO_2 hydrogenation processes. The list of catalysts taken from literature is represented in Table 3 SM in the Supplementary material.

These findings underscore the potential of MgCuFe-US and MgCuFe-BM catalysts in the context of sustainable and cost-effective Fischer-Tropsch synthesis. They offer a competitive alternative to traditional catalysts, balancing performance with economic feasibility, which is crucial for industrial applications. Future enhancements, possibly through modification of synthesis methods or compositional tuning, could bridge the gap in performance with high-end metallosilicates, while maintaining the advantages of lower cost and simpler synthesis associated with hydrotalcite-based catalysts.

4. Conclusions

In this study we synthesized new Fe-based hydrotalcites and used them as catalysts in both Fischer–Tropsch synthesis and CO_2 hydrogenation. We examined the catalytic activity of the materials under different temperatures by using two distinct synthesis routes: ball milling and ultrasonic processing. Our studies showed that specific preparation procedure significantly influences catalytic the activity of the materials and that it is temperature dependent.

Both MgCuFe-BM and MgCuFe-US catalysts demonstrated comparable CO conversion capacity at higher temperatures, but they exhibited different product distribution, primarily due to different pore size distribution. However, under 250 °C, the ultrasound processed Fe-based catalyst exhibited roughly 10% higher catalytic activity. Similar trends were observed for CO_2 hydrogenation, with the MgCuFe-US catalysts showing higher selectivity for C_{7+} hydrocarbons in all evaluated temperatures, while the MgCuFe-BM catalysts showed higher selectivity for C_{2-6} hydrocarbons.

The experiments conducted at 300 °C yielded the greatest C_{2+} production and conversions (up to 98.5%) among the reactions carried out at various temperatures for both CO and CO_2 feeds. This resulted in 50.2% for the ball milled sample and 51.3% for the ultrasound-processed sample in the case of CO hydrogenation. Interestingly, during CO_2 hydrogenation, the MgCuFe-US sample

maintained a higher alpha value, indicating a higher selectivity towards longer chain hydrocarbons compared to the MgCuFe-BM sample.

Our study offers promising insights into the performance of iron-based hydrotalcite catalysts in both CO and CO_2 hydrogenation reactions, suggesting a versatile utility for such catalysts in diverse application conditions. Following these encouraging findings, further research will be conducted on this class of hydrotalcite catalysts in different CO_2/H_2 feed ratios and conditions to further explore and optimize their potential in sustainable chemical production.

CRediT authorship contribution statement

Arian Grainca: Investigation, Validation and Writing; **Elisa Boccalon**: Investigation and Writing **Morena Nochetti:** Conceptualization, Methodology, Writing; **Alessandro Di Michele**: Supervision, Investigation and Writing; **Mariangela Longhi**: Methodology, Writing, Carlo **Pirola**: Conceptualization, Methodology, Writing.

Declaration of Competing Interest

The authors declare that they have no known competing financial interests or personal relationships that could have appeared to influence the work reported in this paper.

Acknowledgments

This work has been partially funded by the European Union - NextGenerationEU under the Italian Ministry of University and Research (MUR) National Innovation Ecosystem grant ECS00000041 - VITALITY. This work has been partially funded by Piano di Sostegno alla Ricerca (PSR 2021-22), Action A of the Dipartimento di Chimica, Università degli Studi di Milano and by the Project PNRR PE2 NEST (Network 4 Energy Sustainable Transition)

Moreover, Authors thank Prof. Michela Signoretto, Prof. Elena Ghedini and Prof. Federica Menegazzo of University of Venezia for TPR analysis reported in the Supplemental Material.

References

[1] Sun X, Atiyeh HK, Li M, Chen Y. Biochar facilitated bioprocessing and biorefinery for productions of biofuel and chemicals: A review. Bioresource Technology 2020;295:122252.

[2] Gholami Z, Tišler Z, Rubáš V. Recent advances in Fischer-Tropsch synthesis using cobalt-based catalysts: A review on supports, promoters, and reactors. Catalysis Reviews 2021;63(3):512-95.

[3] Shahabuddin M, Alam MT, Krishna BB, Bhaskar T, Perkins G. A review on the production of renewable aviation fuels from the gasification of biomass and residual wastes. Bioresource Technology 2020;312:123596.

[4] Zhang Q, Kang J, Wang Y. Development of novel catalysts for Fischer–Tropsch synthesis: tuning the product selectivity. ChemCatChem 2010;2(9):1030-58.

[5] Qi Z, Chen L, Zhang S, Su J, Somorjai GA. A mini review of cobalt-based nanocatalyst in Fischer-Tropsch synthesis. Applied Catalysis A: General 2020;602:117701.

[6] Stavitskaya A, Mazurova K, Kotelev M, Eliseev O, Gushchin P, Glotov A, et al. Ruthenium-loaded halloysite nanotubes as mesocatalysts for Fischer–Tropsch synthesis. Molecules 2020;25(8):1764.

[7] Choi YH, Jang YJ, Park H, Kim WY, Lee YH, Choi SH, et al. Carbon dioxide Fischer-Tropsch synthesis: A new path to carbon-neutral fuels. Applied catalysis B: environmental 2017;202:605-10.

[8] Porosoff MD, Yan B, Chen JG. Catalytic reduction of CO 2 by H 2 for synthesis of CO, methanol and hydrocarbons: challenges and opportunities. Energy & Environmental Science 2016;9(1):62-73.

[9] Nishimura S, Takagaki A, Ebitani K. Characterization, synthesis and catalysis of hydrotalcite-related materials for highly efficient materials transformations. Green Chemistry 2013;15(8):2026-42.

[10] Lima-Corrêa RA, Castro CS, Damasceno AS, Assaf JM. The enhanced activity of base metal modified MgAl mixed oxides from sol-gel hydrotalcite for ethylic transesterification. Renewable Energy 2020;146:1984-90.

[11] Homsi D, Rached JA, Aouad S, Gennequin C, Dahdah E, Estephane J, et al. Steam reforming of ethanol for hydrogen production over Cu/Co-Mg-Al-based catalysts prepared by hydrotalcite route. Environmental Science and Pollution Research 2017;24:9907-13.

[12] Rivas M, Fierro J, Guil-Lopez R, Pena M, La Parola V, Goldwasser M. Preparation and characterization of nickel-based mixed-oxides and their performance for catalytic methane decomposition. Catalysis Today 2008;133:367-73.

[13] Forgionny A, Fierro J, Mondragón F, Moreno A. Effect of Mg/Al Ratio on catalytic behavior of Fischer–Tropsch cobalt-based catalysts obtained from hydrotalcites precursors. Topics in catalysis 2016;59:230-40.

[14] Jung J-S, Hong GH, Park JI, Yang E-H, Hodala JL, Moon DJ. Effect of cobalt supported on meso–macro porous hydrotalcite in Fischer–Tropsch synthesis. RSC advances 2016;6(106):104280-93.

[15] Tsai Y-T, Mo X, Campos A, Goodwin Jr JG, Spivey JJ. Hydrotalcite supported Co catalysts for CO hydrogenation. Applied Catalysis A: General 2011;396(1-2):91-100.

[16] Manzoli M, Bonelli B. Microwave, ultrasound, and mechanochemistry: unconventional tools that are used to obtain “smart” catalysts for CO2 hydrogenation. Catalysts 2018;8(7):262.

[17] Pirola C, Bianchi C, Di Michele A, Diodati P, Boffito D, Ragaini V. Ultrasound and microwave assisted synthesis of high loading Fe-supported Fischer–Tropsch catalysts. Ultrasonics sonochemistry 2010;17(3):610-6.

[18] Chatel G. Sonochemistry in nanocatalysis: the use of ultrasound from the catalyst synthesis to the catalytic reaction. Current opinion in green and sustainable chemistry 2019;15:1-6.
[19] Ragaini V, Pirola C, Borrelli S, Ferrari C, Longo I. Simultaneous ultrasound and microwave new reactor: detailed description and energetic considerations. Ultrasonics Sonochemistry 2012;19(4):872-6.
[20] Sun X, Kang CH, Park JJ, Kim HS, Om AS, Yoon JY. An experimental study on the thermal performance of a novel hydrodynamic cavitation reactor. Experimental Thermal and Fluid Science 2018;99:200-10.
[21] Kim B, Won J, Duran JA, Park LC, Park SS. Investigation of sonochemical treatment of heavy hydrocarbon by ultrasound-assisted cavitation. Ultrasonics Sonochemistry 2020;68:105216.
[22] Mendoza HR, Jordens J, Pereira MVL, Lutz C, Van Gerven T. Effects of ultrasonic irradiation on crystallization kinetics, morphological and structural properties of zeolite FAU. Ultrasonics Sonochemistry 2020;64:105010.
[23] Boccalon E, Viscusi G, Sorrentino A, Marmottini F, Nocchetti M, Gorrasi G. Solvent-free synthesis of halloysite-layered double hydroxide composites containing salicylate as novel, active fillers. Colloids and Surfaces A: Physicochemical and Engineering Aspects 2021;627:127135.
[24] Khadim AT, Albayati TM, Saady NMC. Removal of sulfur compounds from real diesel fuel employing the encapsulated mesoporous material adsorbent Co/MCM-41 in a fixed-bed column. Microporous and Mesoporous Materials 2022;341:112020.
[25] Chen Y, Wei J, Duyar MS, Ordomsky VV, Khodakov AY, Liu J. Carbon-based catalysts for Fischer–Tropsch synthesis. Chemical Society Reviews 2021;50(4):2337-66.
[26] Ali NS, Salih IK, Harharah HN, Majdi HS, Salih HG, Kalash KR, et al. Utilization of Loaded Cobalt onto MCM-48 Mesoporous Catalyst as a Heterogeneous Reaction in a Fixed Bed Membrane Reactor to Produce Isomerization Product from n-Heptane. Catalysts 2023;13(7):1138.
[27] Di Fronzo A, Pirola C, Comazzi A, Galli F, Bianchi C, Di Michele A, et al. Co-based hydrotalcites as new catalysts for the Fischer–Tropsch synthesis process. Fuel 2014;119:62-9.
[28] Lu F, Chen X, Lei Z, Wen L, Zhang Y. Revealing the activity of different iron carbides for Fischer-Tropsch synthesis. Applied Catalysis B: Environmental 2021;281:119521.
[29] Riedel T, Claeys M, Schulz H, Schaub G, Nam S-S, Jun K-W, et al. Comparative study of Fischer–Tropsch synthesis with H2/CO and H2/CO2 syngas using Fe-and Co-based catalysts. Applied Catalysis A: General 1999;186(1-2):201-13.
[30] Previtali D, Longhi M, Galli F, Di Michele A, Manenti F, Signoretto M, et al. Low pressure conversion of CO2 to methanol over Cu/Zn/Al catalysts. The effect of Mg, Ca and Sr as basic promoters. Fuel 2020;274:117804.
[31] Pirola C, Scavini M, Galli F, Vitali S, Comazzi A, Manenti F, et al. Fischer–Tropsch synthesis: EXAFS study of Ru and Pt bimetallic Co based catalysts. Fuel 2014;132:62-70.
[32] Costantino U, Ambrogi V, Nocchetti M, Perioli L. Hydrotalcite-like compounds: versatile layered hosts of molecular anions with biological activity. Microporous and Mesoporous Materials 2008;107(1-2):149-60.
[33] Devasahayam S. Catalytic actions of MgCO3/MgO system for efficient carbon reforming processes. Sustainable Materials and Technologies 2019;22:e00122.
[34] Hofer L, Cohn E, Peebles W. The modifications of the carbide, Fe2C; their properties and identification. Journal of the American Chemical Society 1949;71(1):189-95.
[35] Park JC, Yeo SC, Chun DH, Lim JT, Yang J-I, Lee H-T, et al. Highly activated K-doped iron carbide nanocatalysts designed by computational simulation for Fischer–Tropsch synthesis. Journal of Materials Chemistry A 2014;2(35):14371-9.

[36] Hájek M, Tomášová A, Kocík J, Podzemná V. Statistical evaluation of the mutual relations of properties of Mg/Fe hydrotalcites and mixed oxides as transesterification catalysts. Applied Clay Science 2018;154:28-35.
[37] Bardestani R, Patience GS, Kaliaguine S. Experimental methods in chemical engineering: specific surface area and pore size distribution measurements—BET, BJH, and DFT. The Canadian Journal of Chemical Engineering 2019;97(11):2781-91.
[38] Zhang G, Kan X, Zheng Y, Cao Y, Liang S, Xiao Y, et al. A solid thermal and fast synthesis of MgAl-hydrotalcite nanosheets and their applications in the catalytic elimination of carbonyl sulfide and hydrogen sulfide. New Journal of Chemistry 2021;45(7):3535-45.
[39] Moghtada A, Ashiri R. Superiority of sonochemical processing method for the synthesis of barium titanate nanocrystals in contrast to the mechanochemical approach. Ultrasonics Sonochemistry 2018;41:127-33.
[40] Ferrairo BM, Mosquim V, de Azevedo-Silva LJ, Pires LA, Padovini DSS, Magdalena AG, et al. Production of bovine hydroxyapatite nanoparticles as a promising biomaterial via mechanochemical and sonochemical methods. Materials Chemistry and Physics 2023;295:127046.
[41] Alismaeel ZT, Al-Jadir TM, Albayati TM, Abbas AS, Doyle AM. Modification of FAU zeolite as an active heterogeneous catalyst for biodiesel production and theoretical considerations for kinetic modeling. Advanced Powder Technology 2022;33(7):103646.
[42] Yao Y, Liu X, Gorimbo J, Xiong H, Fox J, Glasser D, et al. Fischer-Tropsch synthesis: A long term comparative study of the product selectivity and paraffin to olefin ratios over an iron-based catalyst activated by syngas or H2. Applied Catalysis A: General 2020;602:117700.
[43] Kuz'min A, Dyatlova YN, Tikhov S, Kurkin V, Sadykov V, Slivinskii E, et al. Fischer-Tropsch Catalysts Based on Zr-Fe Intermetallides Encapsulated in an Al 2 O 3/Al Matrix. Kinetics and catalysis 2005;46:743-51.
[44] Grainca A, Sugliani C, Boccalon E, Nocchetti M, Bianchi C, Pirola C. Iron Based Nano-hydrotalcites Promoted with Cu as Catalysts for Fischer-tropsch Synthesis in Biomass to Liquid Process. Chemical Engineering Transactions 2022;96:127-32.
[45] Fan L, Yokota K, Fujimoto K. Supercritical phase fischer-tropsch synthesis: Catalyst pore-size effect. AIChE Journal 1992;38(10):1639-48.
[46] Cabrera-Munguía DA, González H, Tzompantzi F, Gutiérrez-Alejandre A, Solís-Casados DA, Rico JL. New insights on the basicity of ZnAl–Zr hydrotalcites activated at low temperature and their application in transesterification of soybean oil. Journal of Materials Research 2018;33(21):3614-24.
[47] Weiß J, Yang Q, Bentrup U, Kondratenko EV, Brückner A, Kubis C. Operando DRIFT and In situ Raman Spectroscopic Studies on Aspects of CO2 Fischer-Tropsch Synthesis Catalyzed by Bulk Iron Oxide-Based Catalysts. ChemCatChem 2022;14(22):e202200577.
[48] Okoye-Chine CG, Moyo M, Hildebrandt D. Fischer–Tropsch synthesis: The effect of hydrophobicity on silica-supported iron catalysts. Journal of Industrial and Engineering Chemistry 2021;97:426-33.
[49] Barrios AJ, Gu B, Luo Y, Peron DV, Chernavskii PA, Virginie M, et al. Identification of efficient promoters and selectivity trends in high temperature Fischer-Tropsch synthesis over supported iron catalysts. Applied Catalysis B: Environmental 2020;273:119028.
[50] Suo H, Wang S, Zhang C, Xu J, Wu B, Yang Y, et al. Chemical and structural effects of silica in iron-based Fischer–Tropsch synthesis catalysts. Journal of catalysis 2012;286:111-23.
[51] Ali NS, Kalash KR, Ahmed AN, Albayati TM. Performance of a solar photocatalysis reactor as pretreatment for wastewater via UV, UV/TiO2, and UV/H2O2 to control membrane fouling. Scientific Reports 2022;12(1):16782.
[52] Ali NS, Harharah HN, Salih IK, Cata Saady NM, Zendehboudi S, Albayati TM. Applying MCM-48 mesoporous material, equilibrium, isotherm, and mechanism for the effective adsorption of 4-nitroaniline from wastewater. Scientific Reports 2023;13(1):9837.

[53] Geng S, Jiang F, Xu Y, Liu X. Iron-based Fischer–Tropsch synthesis for the efficient conversion of carbon dioxide into Isoparaffins. ChemCatChem 2016;8(7):1303-7.
[54] Jiang F, Liu B, Geng S, Xu Y, Liu X. Hydrogenation of CO 2 into hydrocarbons: enhanced catalytic activity over Fe-based Fischer–Tropsch catalysts. Catalysis Science & Technology 2018;8(16):4097-107.
[55] Visconti CG, Martinelli M, Falbo L, Infantes-Molina A, Lietti L, Forzatti P, et al. CO2 hydrogenation to lower olefins on a high surface area K-promoted bulk Fe-catalyst. Applied Catalysis B: Environmental 2017;200:530-42.
[56] Wang J, You Z, Zhang Q, Deng W, Wang Y. Synthesis of lower olefins by hydrogenation of carbon dioxide over supported iron catalysts. Catalysis today 2013;215:186-93.
[57] Liu J, Zhang A, Jiang X, Liu M, Sun Y, Song C, et al. Selective CO2 hydrogenation to hydrocarbons on Cu-promoted Fe-based catalysts: dependence on Cu–Fe interaction. ACS sustainable chemistry & engineering 2018;6(8):10182-90.
[58] Gu H, Ding J, Zhong Q, Zeng Y, Song F. Promotion of surface oxygen vacancies on the light olefins synthesis from catalytic CO2 hydrogenation over FeK/ZrO2 catalysts. international journal of hydrogen energy 2019;44(23):11808-16.
[59] Cui X, Gao P, Li S, Yang C, Liu Z, Wang H, et al. Selective production of aromatics directly from carbon dioxide hydrogenation. ACS Catalysis 2019;9(5):3866-76.